Catalytically Activated Palladium@Platinum Nanowires for Accelerated Hydrogen Gas Detection

Xiaowei Li,[†] Yu Liu,[‡] John C. Hemminger,[§] and Reginald M. Penner*[,†,§]

[†]Department of Chemical Engineering and Materials Science, [‡]Department of Physics, and [§]Department of Chemistry, University of California, Irvine, California 92697-2700, United States

ABSTRACT Platinum (Pt)-modified palladium (Pd) nanowires (or Pd@Pt nanowires) are prepared with controlled Pt coverage. These Pd@Pt nanowires are used as resistive gas sensors for the detection of hydrogen gas in air, and the influence of the Pt surface layer is assessed. Pd nanowires with dimensions of 40 nm (h) × 100 nm (w) × 50 μm (l) are first prepared using lithographically patterned nanowire electrodeposition. A thin Pt surface layer is electrodeposited conformally onto a Pd nanowire at coverages, θ_{Pt}, of 0.10 monolayer (ML), 1.0 ML, and 10 ML. X-ray photoelectron spectroscopy coupled with scanning electron microscopy and electrochemical measurements is consistent with a layer-by-layer deposition mode for Pt on the Pd nanowire surface. The resistance of a single Pd@Pt nanowire is measured during the exposure of these nanowires to pulses of hydrogen gas in air at concentrations ranging from 0.05 to 5.0 vol %. Both Pd nanowires and Pd@Pt nanowires show a prompt and reversible increase in resistance upon exposure to H_2 in air, caused by the conversion of Pd to more resistive PdH_x. Relative to a pure Pd nanowire, the addition of 1.0 ML of Pt to the Pd surface alters the H_2 detection properties of Pd@Pt nanowires in two ways. First, the amplitude of the relative resistance change, $\Delta R/R_0$, measured at each H_2 concentration is reduced at low temperatures (T = 294 and 303 K) and is unaffected at higher temperatures (T = 316, 344, and 376 K). Second, response and recovery rates are both faster at all temperatures in this range and for all H_2 concentrations. For higher θ_{Pt} = 10 ML, sensitivity to H_2 is dramatically reduced. For lower θ_{Pt} = 0.1 ML, no significant influence on sensitivity or the speed of response/recovery is observed.

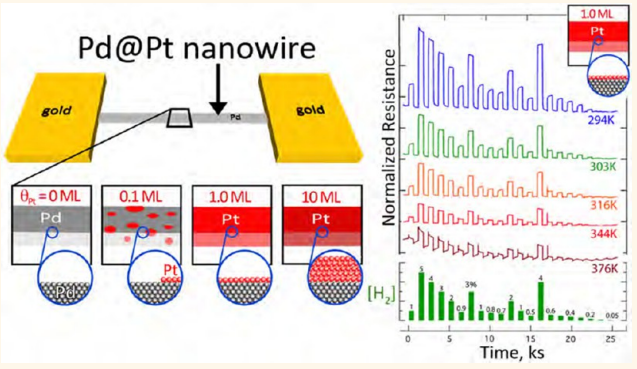

KEYWORDS: electrodeposition · lithography · chemiresistor · palladium · safety · sensor · catalytic

Rapid and sensitive detection of leaked hydrogen gas in air remains technologically challenging.[1−5] The U.S. Department of Energy (DOE) has defined performance metrics including the response and recovery speed, sensitivity, limit of detection (LOD_{H_2}), and the cost (<$40/unit) as well as other attributes (Table 1).[6] The cost requirement constrains the technologies that can be explored in these sensors. One attractive option is palladium and palladium alloy resistors, first demonstrated by Hughes and Schubert in 1992.[7] When these DOE metrics were published in 2009, no H_2 sensor was capable of achieving all of them, and this remains the case today, but nanoscience has enabled considerable progress with resistor-based sensors for H_2. Among the most challenging of the metrics summarized in Table 1 are the response and recovery times: A response time for H_2 exposure of <1 s at 4% H_2 and <60 s at 1% is required in ambient air as is a recovery time of less than 60 s, independent of H_2 concentration. Single palladium (Pd) nanowires,[8−16] films of Pd nanoparticles,[17−19] Pd nanowire networks,[18,20] and Pd structures with engineered nanogaps[21,22] have accelerated sensor response and recovery speed (Table 2), but in most cases, these advances have been demonstrated for H_2 sensing in a background of N_2, not air.[9−11,14,16−18,20−23] (Table 2).

Hydrogen safety sensors must function in air, a much more challenging ambient environment for H_2 sensing than N_2. For example, we[9,11] reported that single Pd nanowires operating at 300 °K in N_2

* Address correspondence to rmpenner@uci.edu.

Received for review January 14, 2015 and accepted February 13, 2015.

Published online February 13, 2015
10.1021/acsnano.5b00302

showed a LOD_{H_2} of 2 ppm and response/recovery times of 40 s/300 s for exposure to 0.10% H_2. However, for a similar Pd nanowire operating in dry air,[9,11] LOD_{H_2} was increased to 100 ppm, and response/recovery times were increased to 400 s/1000 s. The deleterious influence of air can be rationalized as follows: In the N_2 ambient, dihydrogen physisorbs onto the Pd surface, dissociates, and chemisorbs, forming Pd−H (Figure 1):

$$H_2(g) \rightarrow H_2(ads) \quad (1)$$

$$Pd + \frac{1}{2} H_2(ads) \rightarrow Pd - H \quad (2)$$

The electrical resistivity of $PdH_{0.7}$ is almost a factor of 2 higher than that of palladium,[24] allowing the presence of H_2 to be detected as an increase in the resistance of the Pd resistor. Air increases the LOD_{H_2} because the presence of oxygen[25] enables catalytic water formation at the Pd surface, thereby reducing the steady-state surface coverage of chemisorbed hydrogen available to be absorbed into the bulk of the PdH_x (reaction 2 above)[26,27] (Figure 1).

$$Pd - O + \frac{3}{2} H_2(ads) \rightarrow Pd - H + H_2O(ads) \quad (3)$$

$$H_2O(ads) \rightarrow H_2O(g) \quad (4)$$

Chemisorbed oxygen (reaction 3) also blocks Pd adsorption sites, impeding hydrogen adsorption and extending the time required for equilibration of hydrogen in the gas phase with the PdH_x, retarding both response and recovery. The strong influence of oxygen

TABLE 1. Department of Energy Target Metrics Governing Performance for Hydrogen Gas Sensors[a]

parameter	DOE target
sensitivity	25% (1 vol % of H_2)
range and accuracy	0.1−4%, ±1% of full scale over the lifetime of the sensor
lifetime	5 years
response time	<1 min at 25% LFL[b] (1 vol %)
	<1 s at 100% LFL (4 vol %)
recovery time	60 s

[a] Source: DOE Energy Efficiency & Renewable Energy 2009 Hydrogen Sensor Workshop. [b] LFL = Lower flammability limit.

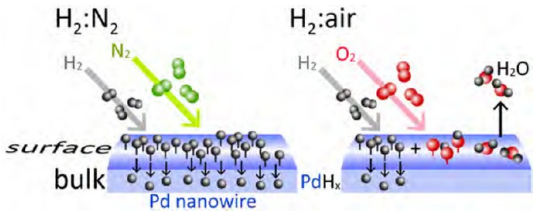

Figure 1. Schematic representation of the influence of oxygen in air on the response of a Pd nanowire to H_2. The sensitivity of the nanowire resistance to H_2 and the speed of the response and recovery of the resistance are reduced in air as compared with N_2.

TABLE 2. Performance Metrics for Fast, Resistance-Based Hydrogen Sensors Operating in Nitrogen and Air

sensing element[a]	critical dimensions	temp (K)	τ_{resp}/τ_{rec} [H_2] ≈ 0.1%[b]	τ_{resp}/τ_{rec} [H_2] ≈ 4%[c]	LOD_{H_2}	ref
			in nitrogen			
fractured Pd nanowire	d = 200−250 nm	rt	nr	0.07 s/0.07 s	1−2%	14,16
Pd film nanogap	t = 10−100 nm	rt	nr	52 s/122 s	2%	21
Pd nanowire	d = 50−80 nm	rt	15 s/nr	12 s/nr	27 ppm	8
Pd film nanogap	t = 6−10 nm	rt	nr	0.5 s/0.5 s	1−2%	23
Pd film nanogap	t = ∼10 nm	rt	nr	5−10 s/200 s	0.5%	22
Pd nanoparticle film	t = 3.3 nm	rt	10 s/10 s	0.07 s/0.07 s	25 ppm	17
Pd nanowire	33 (h) × 47 nm (w)	rt	40 s/300 s	30 s/100 s	2 ppm	9,11
Pd nanowire	27 (h) × 75 nm (w)	428	7 s/15 s	2 s/6 s	200 ppm	10
Pd nanonetwork	d = 1−3 nm	rt	30 s/nr	3−4 s/nr	1000 ppm	18,20
			in air			
Pd/Ni film	t = 50 nm	rt	120 s/20 s	20 s/100 s	nr	7
Pd nanowire	d = 50−80 nm	rt	nr	nr	1000 ppm	8
Pd nanowire	25(h) × 85 nm (w)	rt	400 s/1000 s	100 s/200 s	100 ppm	9,11
Pt nanowire[d]	20 (h) × 130 nm (w)	550	150 s/1100 s	1 s/1100 s	10 ppm	13
			Pd@Pt nanowires			
θ_{Pt} = 0 ML	40 (h) × 100 nm (w)	294	450 s/480 s	80 s/380 s	500 ppm	this work
	〃	376	nr	4.5 s/10 s	1%	〃
θ_{Pt} = 0.1 ML	〃	294	150 s/1100 s	80 s/380 s	500 ppm	〃
	〃	376	nr	4 s/10 s	1%	〃
θ_{Pt} = 1.0 ML	〃	294	250 s/15 s	35 s/50 s	0.2%	〃
	〃	376	nr	2 s/2.5 s	0.4%	〃
θ_{Pt} = 10 ML	〃	294	nr	40 s/40 s	0.9%	〃
	〃	376	nr	3 s/2.5 s	2%	〃

[a] Abbreviations: rt = room temperature, t = thickness, d = diameter, (h) × (w) are the lateral dimensions of a nanowire with a rectangular cross section, nr = not reported. [b] $R_{initial}$ to 0.90R_{max} response time. [c] R_{max} to 0.10R_{max} recovery time. [d] Pt nanowire does not discriminate concentration across its entire response range.

on the sensing behavior of Pd nanowires shows that surface chemistry is a critical factor in determining the performance of resistance-based hydrogen gas sensors.

One tactic for accelerating response and recovery in both air and N_2 is to heat a Pd nanowire.[10] At a Pd nanowire, both response to H_2 and recovery from it are strongly thermally activated.[10] But even after optimization of the elevated nanowire temperature at 428 K, the resulting performance (Table 2) does not meet the requirements summarized in Table 1. An obvious place to look for an additional improvement is the nanowire surface chemical composition.

The formation of a Pt shell on a Pd nanowire has the potential to favorably alter the surface chemistry of a Pd nanowire. Johannson *et al.*[28] have shown that in dry air at T = 100 °C, Pt is a better catalyst than Pd for reaction 3. Pt is also a superior catalyst for reaction 2, which is the rate-limiting reaction for sensor response in N_2.[10] We[13] recently prepared platinum nanowires and evaluated their performance as hydrogen sensors. To our surprise, we found dramatic increases in response speed for sensors based on Pt nanowires but even slower sensor recovery as compared with Pd nanowires of the same size.[13] For example, for a Pt nanowire operating in air at 550 K, the response time was decreased by a factor of 100 at 1.0% H_2, while under identical conditions, the recovery time was slower than for a Pd nanowire of identical size by a factor of 14 (1000 s *versus* 70 s).[13]

Here, we assess the influence of ultrathin Pt layers, corresponding to a Pt coverage, θ_{Pt}, of 0.10 to 10 ML, on the hydrogen sensing performance of a Pd nanowire in air. Pt layers were prepared by electrodeposition under conditions that promote a layer-by-layer deposition mode for platinum onto the Pd nanowire surface. We find that the Pt layer accelerates both the response and recovery to hydrogen in air. Importantly, Pt increases the limit of detection for hydrogen (LOD_{H_2}) at room temperature but extends it to lower values at elevated temperatures of 376 K, enabling simultaneous acceleration of response/recovery with virtually no degradation of the sensitivity to H_2. The net effect is that, for an optimum Pt coverage of θ_{Pt} = 1.0 ML, the H_2 sensing performance in air of a Pd@Pt nanowire operating at T = 376 K is significantly improved relative to pure Pd nanowire—the current state-of-the-art—operating anywhere in the temperature range from 294 to 376 K.

RESULTS AND DISCUSSION

Preparation and Characterization of Platinum-Modified Palladium Nanowires. Palladium nanowires with lateral dimensions of 40 nm (h) × 100 nm (w) and lengths of more than 100 μm were prepared using lithographically patterned nanowire electrodeposition (LPNE) as previously described.[9−12,29] Gold electrical contacts were then patterned using photolithography, metal evaporation, and liftoff to electrically address a 50 μm section of this nanowire (Figure 2a). These contacts were covered with a photoresist layer to insulate them from contact with the platinum plating solution and the dilute, aqueous H_2SO_4 electrolyte used for electrochemical nanowire characterization.

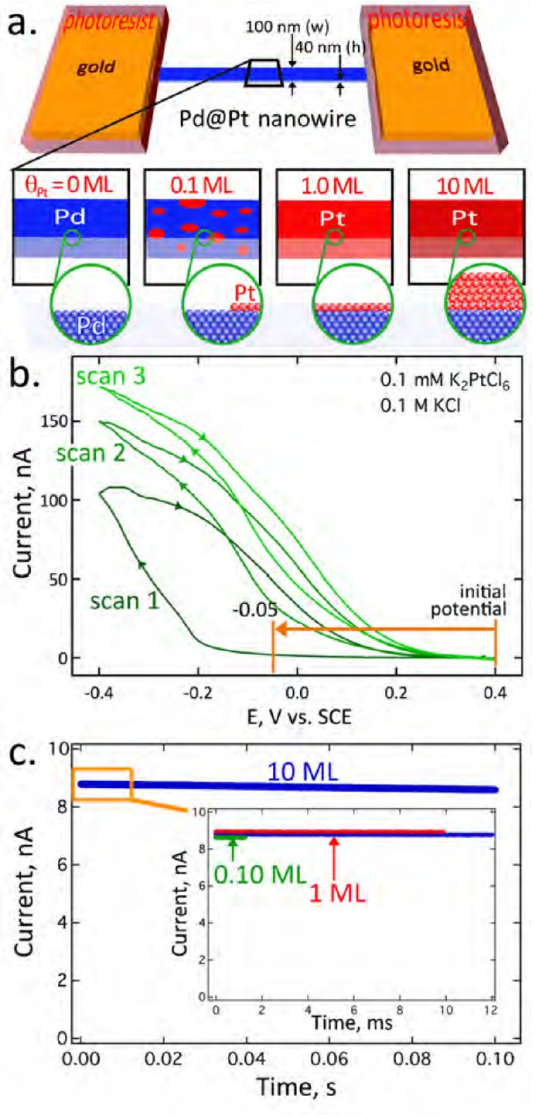

Figure 2. Electrodeposition of Pt on a Pd nanowire. (a) Pd@Pt nanowires were prepared by electrodepositing controlled quantities of Pt, based upon deposition charge, onto a single Pd nanowire prepared using LPNE, as shown schematically here. (b) Cyclic voltammetry of a Pd nanowire in aqueous 0.1 mM K_2PtCl_6, 0.1 M KCl. Platinum metal was electrodeposited from aqueous KCl solution at −0.05 V *vs* saturated calomel electrode (SCE). Under these deposition conditions, layer-by-layer deposition of Pt is expected, as indicated schematically in (a). (c) Current *versus* time transients showing a constant Pt deposition current as a function of time, as expected for a kinetically-controlled layer-by-layer deposition mechanism. The deposition charge associated with the electrodeposition of a Pt monolayer from a solution of $PtCl_6^{2-}$ is 832 μQ/cm^2.

Surface-limited redox replacement (SLRR) is an elegant method for electrodepositing monolayer quantities of a noble metal on the surface of another

noble metal.[30−32] SLRR is a two-step process involving the under-potential deposition of a monolayer of a non-noble metal (*e.g.*, Cu) onto a noble metal electrode (*e.g.*, Pd) followed by galvanic replacement[33−35] of the Cu by a noble metal such as Pt. In contrast, for the particular system of interest here (Pt on Pd), instead of using an SLRR method, we have used a single over-potential step to grow Pt in a layer-by-layer fashion on the palladium nanowire. This was accomplished by stepping the potential of the nanowire from +0.40 V to −0.050 V *vs* saturated calomel reference electrode (SCE) in a solution containing 0.1 mM K_2PtCl_6 in 0.10 M KCl. As shown in the cyclic voltammogram in Figure 2b, −0.050 V is well positive of the potential, where a rapid increase in the reduction current signals the onset of nucleation of three-dimensional Pt islands on the Pd surface (∼−0.20 V). At potentials positive of this onset, our data indicate that the electrodeposition of Pt occurs by a layer-by-layer process as detailed below.

A layer-by-layer, or Frank−Van der Merwe,[36] growth mechanism for Pt deposition onto the Pd nanowire is supported by three experimental observations: First, the deposition current is constant as a function of time (Figure 2c). This behavior has also been seen previously for Pt on Pd electrodeposition[37] as well as for other metal-on-metal deposition systems at low overpotentials.[38,39] At higher overpotentials (more negative deposition potentials), layer-by-layer growth is replaced by the growth of three-dimensional metal nuclei.[37−39] This Volmer−Webber growth mode[36] is characterized by a peak-shaped current *versus* time response that is diagnostic of either instantaneous or progressive nucleation of three-dimensional nuclei.[40−42] Second, no three-dimensional nuclei are observed in scanning electron microscopy (SEM) images of these nanowires acquired after Pt deposition, for any of the Pt coverages examined here, at any magnification (*e.g.*, Figure 3e). Such particles should be observed if the three-dimensional growth of Pt on the Pd surface is occurring. Moreover, energy-dispersive X-ray spectroscopy (EDX) elemental maps (Figure 3g) show that the deposited Pt is uniformly distributed on the surface of a Pd@Pt nanowire with θ_{Pt} = 10 ML, as expected for the deposition of conformal Pt layers. Third, X-ray photoelectron spectroscopy (XPS) analysis for Pd and Pt (Figure 4) shows a strong, linear decrease in the Pd photoelectron signal with the deposition of 10 and 20 ML of Pt onto clean Pd nanowire surfaces. This attenuation of the Pd XPS signal is only expected if the Pd surface is covered by a conformal Pt layer. In contrast, a weaker, nonlinear attenuation of the Pd XPS signal is expected with Pt deposition if prompt, three-dimensional nucleation and growth of Pt is occurring.

It is important to appreciate that the alloying of the electrodeposited Pt with Pd is possible, in principle. Both Pd and Pt are detected by XPS for θ_{Pt} = 20 ML (Figure 4), but the abruptness of the Pd/Pt interface cannot be discerned from these data.

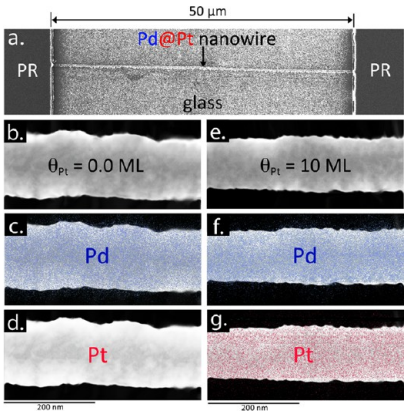

Figure 3. SEM and EDX analysis of Pd and Pd@Pt (10 ML) nanowires. (a) Low-magnification SEM image of a single nanowire H_2 sensor showing the photoresist (PR)-covered gold contacts. (b−d) Pd nanowire with no deposited Pt. (e−g) Pd@Pt nanowire with θ_{Pt} = 10 ML. Shown are (b,e) secondary electron images, (c,f) EDX elemental map for Pd superimposed on the image of (b), (d,g) EDX elemental map for Pt superimposed on the image of (e).

Finally, with increasing θ_{Pt}, the cyclic voltammetry of Pd@Pt nanowires in aqueous 0.050 M H_2SO_4 shows the emergent characteristics of a surface Pt layer (Figure 5a). Specifically, the peak current for the oxide reduction (≈0.75 V *vs* RHE, reversible hydrogen electrode) decreases as Pt is deposited on the Pd surface, and the peak potential of this oxide peak shifts positive as previously reported (Figure 5b).[43−45] The catalytic activity of the surface for proton reduction at ≈0.20 V (Figure 5a) also increases with θ_{Pt}, in agreement with previous observations.[43] The smooth evolution of the cyclic voltammetry of these nanowires with increasing θ_{Pt} does not prove that Pt is deposited in a layer-by-layer fashion, but it does indicate that the electrocatalytic properties of the nanowires are modified monotonically with increasing Pt coverage, even for the deposition of extremely small amounts of Pt. In the following, we exploit the modified catalytic properties of Pd@Pt nanowires for H_2 gas detection in air.

Detection of Hydrogen in Air. The temperature-dependent properties of Pd and Pd@Pt nanowires for the detection of H_2 in air were probed over the temperature range from 294 to 376 K (Figure 6). Elevated nanowire temperatures were achieved by controlled Joule heating of the nanowire. Joule heating was effected by increasing the applied voltage to the nanowire, thereby increasing the current, *i*, and causing the dissipation of the resulting i^2R as heat. The temperature of the nanowire was determined with ±1 K accuracy from its electrical resistance in the absence of hydrogen. Calibration of the nanowire resistance with temperature is described in the Methods section. The resistance *versus* time

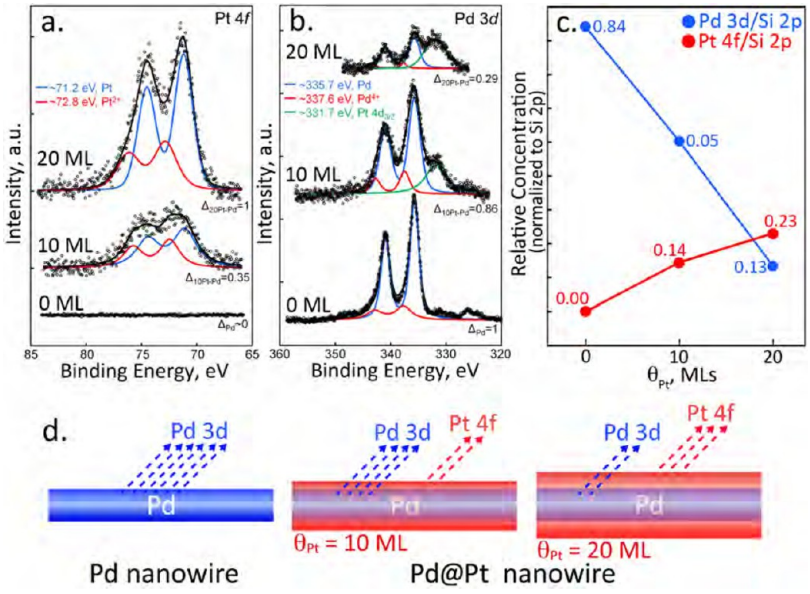

Figure 4. XPS analysis of Pd@Pt nanowires. (a) Pt 4f spectra at θ_{Pt} = 0, 10, and 20 ML showing a buildup of intensity with coverage. (b) Pd 3d XPS spectra ($3d_{3/2}$ at 340 eV and $3d_{5/2}$ at 335 eV) at the same θ_{Pt} values as in (a), showing strong attenuation of the Pd 3d photoelectrons with the deposition of Pt. (c) Integrated intensity *versus* θ_{Pt} for Pt 4f and Pd 3d photoelectrons showing linear increase and decrease, respectively, of the photoelectron intensity.

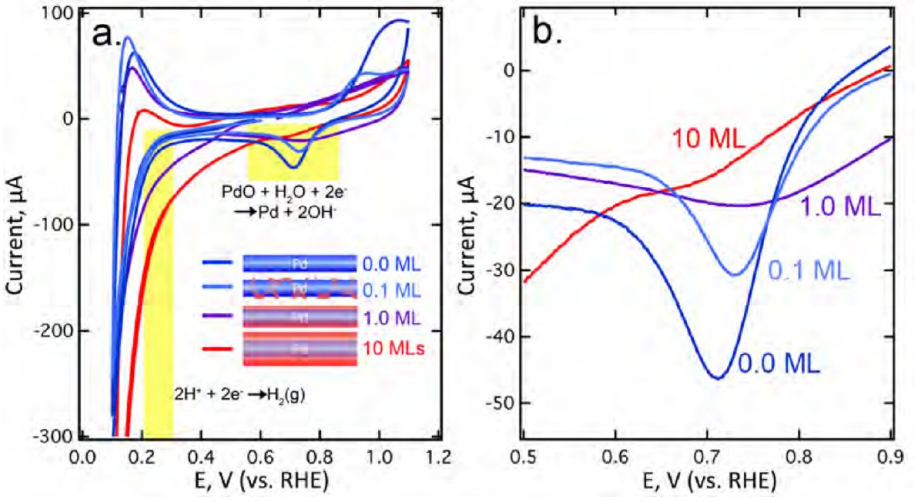

Figure 5. Voltammetry of arrays of Pd nanowires and Pd@Pt nanowires. (a) Cyclic voltammograms at 20 mV/s in aqueous 0.050 M H_2SO_2, showing oxide formation (+1.0 V *vs* RHE), oxide reduction (0.7−0.8 V), and hydrogen evolution at (−0.20 V). Hydrogen evolution currents at −0.20 V progressively increase in the order θ_{Pt} = 0.0 ≈ 0.1 < 1.0 < 10 ML, qualitatively as expected.[43] (b) Palladium oxide reduction region of the CVs shown in (a), highlighting the increased reduction peak currents in the order θ_{Pt} = 0.0 > 0.1 > 1.0 > 10 ML. A positive shift in the peak potential for oxide reduction with increasing Pt coverage is also observed, as previously documented.[43−45]

performance of a 40 nm × 100 nm Pd nanowire for detecting H_2 in air, for example, is shown in Figure 6a. The sensitivity of this nanowire is excellent at 294 K, but response and recovery times are much too slow relative to DOE metrics outlined in Table 1. Heating the nanowire accelerates both response and recovery, at the cost of some loss of sensitivity (Figure 6a), but even at 344 K, this sensor is not fast enough. The performance of single Pd nanowires for detecting H_2 in N_2[8−12,18,20,46,47] and in air[10,11] is state-of-the-art, and the performance seen in Figure 6a is consistent with this prior published work for Pd nanowire H_2 sensors operating in air.[10,11]

Relative to a pure Pd nanowire, the addition of a Pt layer alters the H_2 detection properties of Pd@Pt nanowires in two ways (Figure 6b,c): First, the amplitude of the relative resistance change, $\Delta R/R_0$ (where R_0 is the initial resistance of the nanowire), measured at each H_2 concentration is reduced at low temperatures (T = 294 and 303 K), whereas $\Delta R/R_0$ at higher temperatures (T = 316, 344, and 376 K) is approximately the same as seen for pure Pd nanowires (Figure 7).

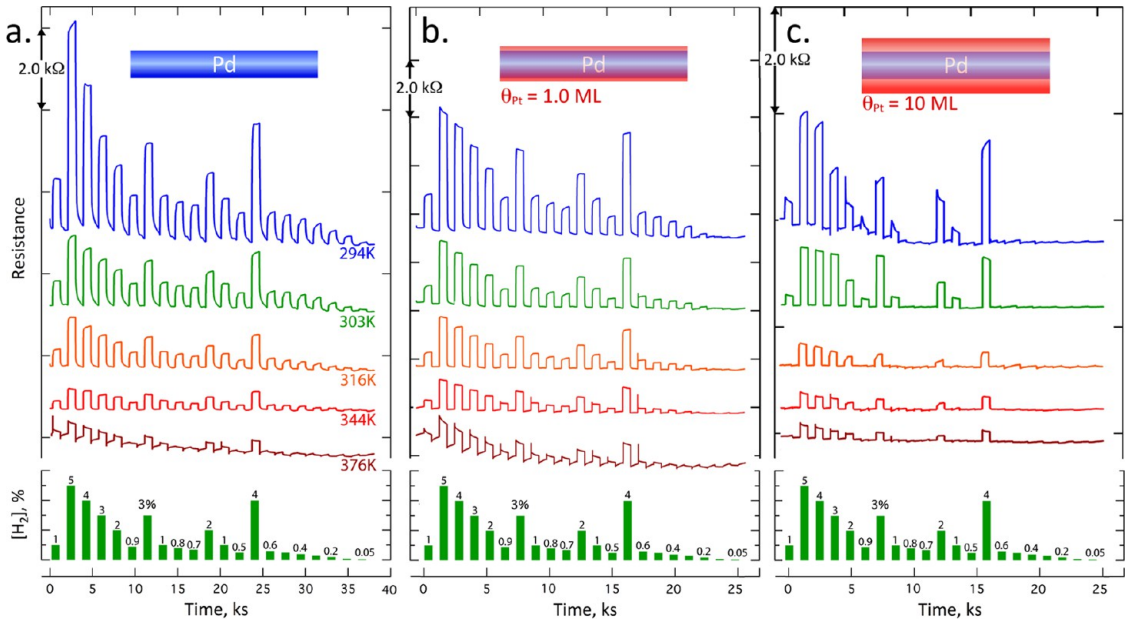

Figure 6. Raw H_2 sensing responses for three nanowires at five temperatures from 294 to 376 K: (a) Pd nanowire with dimensions of 40 nm (h) × 100 nm (w) × 50 μm (l). (b) Pd@Pt nanowire with θ_{Pt} = 1.0 ML. (c) Pd@Pt nanowire with θ_{Pt} = 10 ML. Note that the time scale in (b) and (c) is compressed by 30% relative to (a).

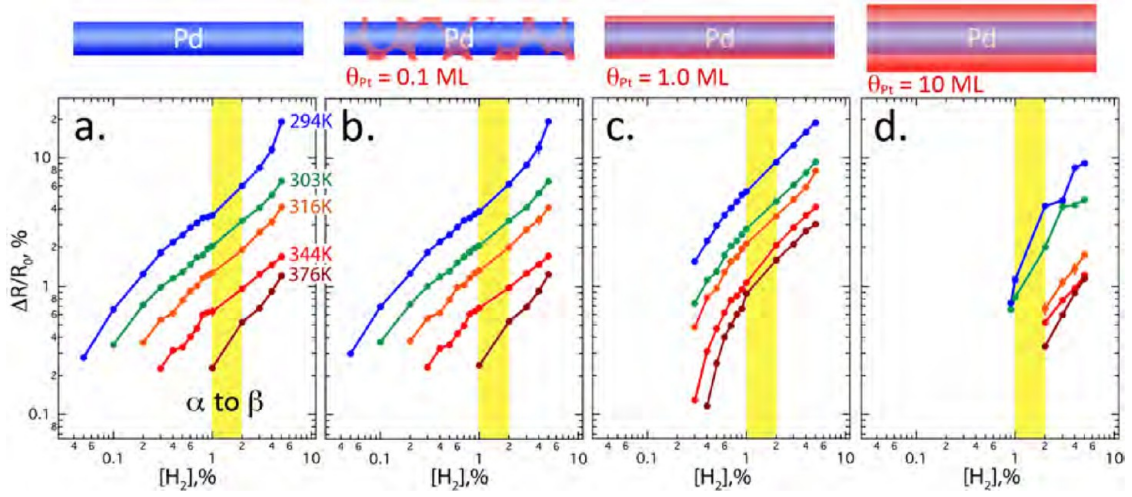

Figure 7. Calibration plots as a function of temperature. Plotted are the normalized resistance change, $\Delta R = R_0$, *versus* [H_2] for (a) pure Pd nanowire, θ_{Pt} = 0 ML, (b) Pd@Pt nanowire with θ_{Pt} = 0.1 ML, (c) Pd@Pt nanowire with θ_{Pt} = 1.0 ML, and (d) Pd@Pt nanowire with θ_{Pt} = 10 ML. The yellow region from 1 to 2% [H_2] coincides with the α-to-β phase transition of PdH_x.

Second, response and recovery rates are accelerated at all temperatures in this range and for all H_2 concentrations (Figures 8 and 9). We discuss both of these effects below.

As shown in Figure 7c, even one atomic layer of Pt causes a loss of sensitivity at 294 and 303 K relative to 0.1 ML of Pt (Figure 7b) or no Pt (Figure 7a). For example, a Pd@Pt nanowire with θ_{Pt} = 1.0 ML shows a LOD_{H_2} of 3000 ppm (T = 294 K), whereas a pure Pd nanowire shows LOD_{H_2} = 500 ppm at the same temperature. At higher temperatures up to 376 K, however, sensitivity disparities disappear: Both a Pd nanowire (Figure 7a) and a Pd@Pt nanowire with θ_{Pt} = 1.0 ML (Figure 7c) show an equal loss in sensitivity to H_2 with increasing T. This heating-induced loss of sensitivity, seen previously for pure Pd nanowires operating in N_2,[8,10] is derived from the reduced solubility of H in Pd.[48,49] For example, the equilibrium hydrogen partial pressure required to attain PdH_x for $0.1 < x < 0.6$ increases by a factor of ≈30 over the range from 294 to 376 K.[48]

Increasing the Pt layer thickness to 10 ML causes a more pronounced loss in sensitivity across all temperatures from 294 to 376 K. A θ_{Pt} = 10 ML Pd@Pt nanowire shows a LOD_{H_2} = 1.0% at 294 K (Figures 6c and 7d) and 2.0% at higher temperatures. Although, as described below, the response and recovery of a Pd@Pt nanowire with a 10 ML Pt surface layer are accelerated, and the

profound loss in sensitivity to H_2 is disabling with respect to the application of this nanowire as a H_2 sensor.

An examination of the raw *R versus* time data of Figure 6b shows that surface Pt can accelerate the response and recovery to H_2 in air for all temperatures in the range from 294 to 376 K, relative to pure Pd (Figure 10). However, θ_{Pt} = 0.1 ML is not enough; these Pd@Pt nanowires show a small but insignificant acceleration of both response and recovery rates (Figure 10). Acceleration of the response and recovery text is significant for both θ_{Pt} = 1.0 and 10 ML Pd@Pt nanowires.

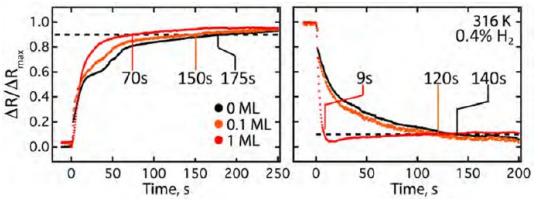

Figure 8. Normalized resistance *versus* time plots for the response (left) and recovery (right) of a Pd nanowire and two Pd@Pt nanowires showing response and recovery times. Shown are data for θ_{Pt} = 0 ML (pure Pd), 0.1 ML, and 1.0 ML as indicated. *T* = 316 K, and the hydrogen concentration is 0.4% in air.

For example, as shown in Figure 10, the addition of 1.0 ML of Pt to the surface of a Pd nanowire accelerates sensor response by a factor of ≈2 across all temperatures and H_2 concentrations (Figure 9c) relative to a pure Pd nanowire (Figure 9a). Recovery of the sensor resistance after H_2 exposure is accelerated by an even larger factor of between 5 at 376 K

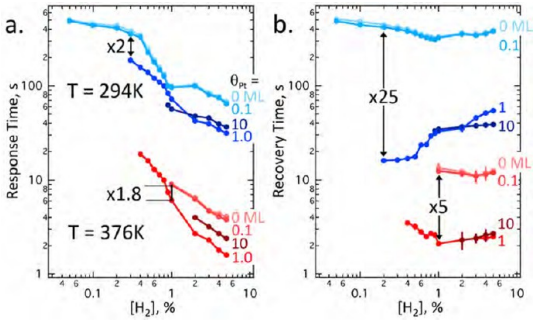

Figure 10. Influence of Pt coverage for Pd@Pt nanowires on the response and recovery of *R* at two temperatures, 294 and 376 K. (a) Response time *versus* [H_2]. The response times at both temperatures are decreased by a factor of ≈2 at the LOD_{H_2} as compared with a pure Pd nanowire operating at the same temperatures. (b) Recovery time *versus* [H_2]. Sensor recovery times are decreased by a factor of 25 at 294 K and by a factor of 5 at 376 K at the LOD_{H_2}.

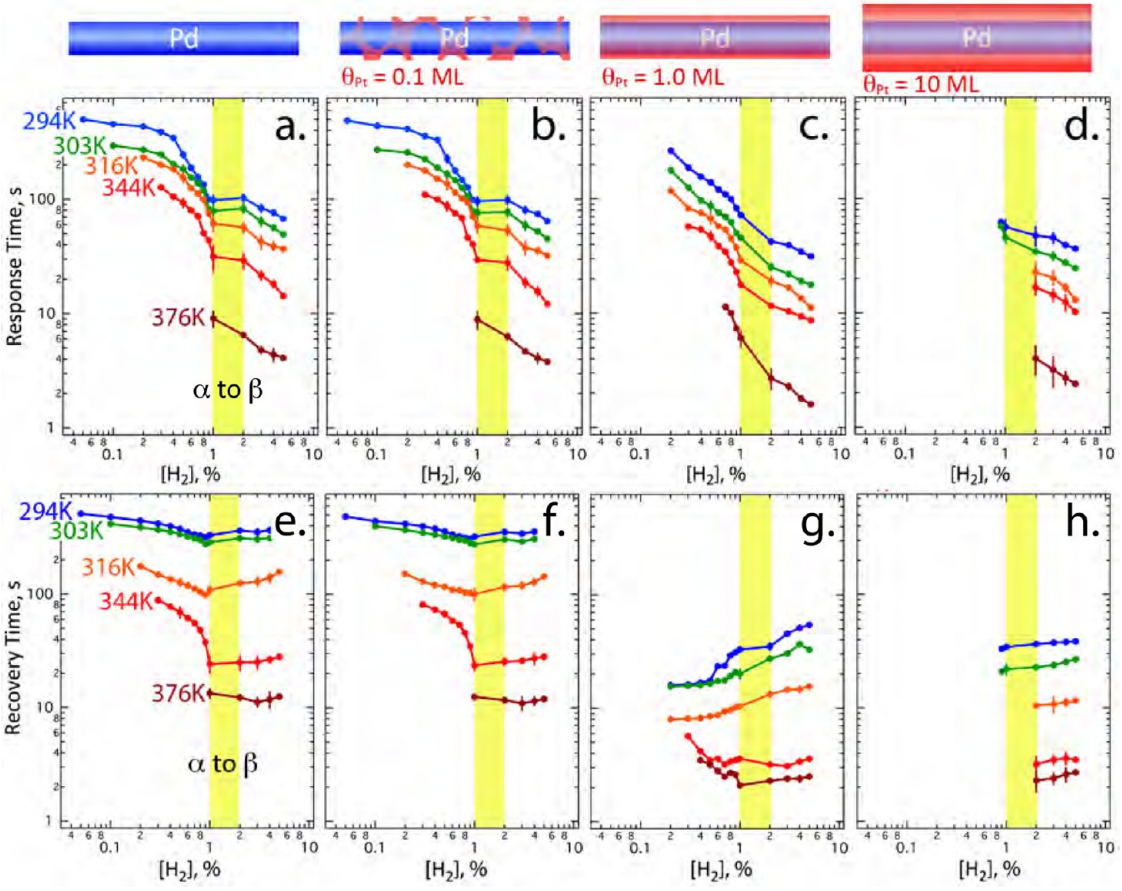

Figure 9. Response (a−d) and recovery (e−h) rate data for four nanowires, at five temperatures, as indicated: (a,e) Pd nanowire, (b,f) Pd@Pt nanowire with θ_{Pt} = 0.1 ML, (c,g) Pd@Pt nanowire with θ_{Pt} = 1.0 ML, and (d,h) Pd@Pt nanowire with θ_{Pt} = 10 ML.

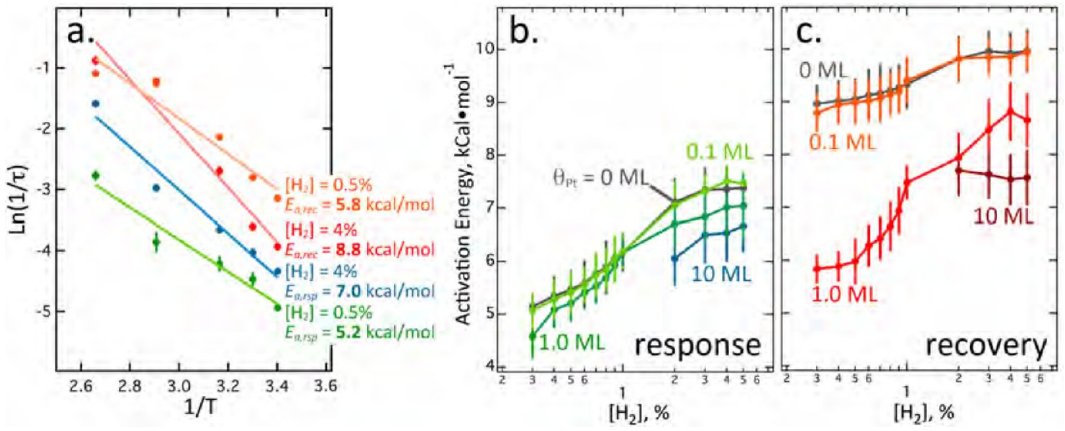

Figure 11. Arrhenius activation energy measurements for sensor response and recovery. (a) Example of Arrhenius plots for the response and recovery of a Pd@Pt nanowire with θ_{Pt} = 1.0 ML at two H_2 concentrations, 4 and 0.5%, as indicated. (b) $E_{a,resp}$ and (c) $E_{a,rec}$ of Pd@Pt nanowire sensors as a function of H_2 concentration in air.

and 20−25 at 294 K (Figure 9g). The comparison of Figure 10 also shows that no significant difference between 1.0 and 10 ML of Pt is seen in either the response (Figure 9c,d) or recovery performance (Figure 9g,h), in spite of the fact that, as already noted, the sensitivity of the 10 ML Pd@Pt nanowire is depressed (Figure 7d).

Like a pure Pd nanowire, the response and recovery of a Pd@Pt nanowire are thermally activated, and both processes are accelerated by Joule heating (Figures 6 and 8).[10] Activation energies for sensor response, $E_{a,resp}$, and recovery, $E_{a,rec}$, can be derived from plots of $\ln(1/\tau)$ *versus* $1/T$ (*e.g.*, Figure 11a), where τ is the response or recovery time, using the Arrhenius equation: $\ln(1/\tau) = -E_a/RT + \ln(A)$. At 376 K, for example, sensor response is accelerated by 1 order of magnitude relative to 294 K across all concentrations—a factor that is nearly identical to that measured for a pure Pd nanowire. $E_{a,resp}$ is unaffected by the platinum surface layer within our experimental error. This suggests that the rate-limiting chemical processes involved in sensor response are unaffected by the Pt surface layer. Since H_2 dissociation is rapid at both Pd and Pt surfaces, the barrier we measure may derive from the transition of a surface hydride species to a bulk hydride. We believe, however, that more rapid water formation by surface Pt is nevertheless responsible for depressing the sensitivity of Pd@Pt nanowires at low T = 294 and 303 K.

In contrast, the $E_{a,rec}$ is strongly influenced by surface Pt. For example, 1.0 ML of Pt causes a significant reduction in $E_{a,rec}$ across all concentrations. At 0.3%, for example, $E_{a,rec}$ is reduced from from 9 kcal/mol for pure Pd to 6 kcal/mol for a Pd@Pt nanowire with θ_{Pt} = 0.1 ML. This reflects a change in the rate-limiting step for recovery at a Pt-covered Pd@Pt nanowire, which is explained by the increased activity of platinum for water formation.

CONCLUSIONS

The response/recovery speed of nanoscale chemical sensors is prone to retardation by rate-limiting surface chemical kinetics because, as the critical dimension of the sensor is reduced, the diffusional flux of molecules to sensor surfaces is increased. Diffusion limits are replaced by kinetic limits for surface chemical reactions that are involved in sensor function. For this reason, the performance of nanoscale sensors should be hypersensitive to catalysts. This paper provides a graphic demonstration of this principle. We have demonstrated that H_2 response and recovery kinetics for a highly optimized H_2 sensor consisting of a Joule-heated Pd nanowire can be significantly accelerated by the addition of minute quantities (*e.g.*, 1 ML) of a Pt metal catalyst to the nanowire surface, altering the kinetics of surface chemical reactions.

Specifically, a Pd@Pt nanowire alters the properties of the Pd nanowire for detecting hydrogen, increasing the response speed by a factor of 2 at the limit of detection and accelerating the recovery of the sensor in air by a factor of 2−25, depending on temperature. These changes apply to a coverage of Pt, θ_{Pt}, of 1.0 ML, the optimum coverage assessed here: A higher θ_{Pt} = 10 ML causes a stronger loss of sensitivity to H_2, making it too insensitive for safety-sensing purposes even though rapid response and recovery seen at the lower Pt coverage are retained. A lower θ_{Pt} = 0.1 ML has no significant influence on sensitivity or the speed of response/recovery, even though this sub-monolayer of Pt does alter the surface electrochemical response of the nanowire (Figure 5). The benchmark that we use for this comparison is a Pd nanowire of the same size, which previously defined the state-of-the-art for resistor-based hydrogen gas detection.[9−11,29]

As a footnote, we also demonstrate that a useful electrochemical method for depositing a conformal monolayer of Pt onto a Pd surface involving the use of very low electrodeposition rates. This process provides an alternative to the well-established surface-limited redox replacement process[30−32] for carrying out the conformal electrodeposition of a noble metal on the surface of another noble metal. Using this approach,

we have electrodeposited ultrathin layers (between 0.1 and 10 ML) of Pt on Pd nanowires to create Pd@Pt core@shell nanowires with enhanced hydrogen gas detection capabilities.

METHODS

Chemicals and Materials. Palladium chloride ($PdCl_2$, 99.999% trace metal basis), potassium hexachloroplatinate(IV) (K_2PtCl_6, 99.99% trace metal basis), ethylenediaminetetraacetic acid (EDTA, 99.995% trace metal basis), and potassium chloride (KCl, 99.3%, ACS certified) were used as received from Sigma-Aldrich. Positive photoresist (Shipley S1808) and developer (Shipley MF-319) were purchased from Microchem Corporation. Acetone, methanol, and nitric acid were used as received from Fisher (ACS certified). Nickel (Ni) and gold (Au) pellets (5 N purity) were used from Kurt J. Lesker Company for evaporation of films. Fast drying silver (Ag) paint was used as received from Ted Pella, Inc. Hydrogen gas (Airgas, purity ≥99.998%) and air (Airgas, purity ≥99.995%) were used as received.

Single Palladium Nanowire Synthesis and Hydrogen Sensor Fabrication. Single palladium nanowires can be synthesized by LPNE as described previously. Nickel films of 40 nm thickness were thermally evaporated onto precleaned 2 in. × 1 in. soda lime glasses, and the thickness of the nickel films was precisely measured by gold quartz crystal microbalance. The following step was to spin-coat a positive photoresist layer (Shipley S1808) at 2500 rmp for 80 s and bake the photoresist in a constant temperature forced convection oven (Yamato Scientific America, Inc., model DKN 600) for 30 min at 90 °C. After the photoresist layer was cooled to room temperature, it was mounted in contact with a quartz photolithographic mask on a photolithographic mask alignment fixture (Newport 83210). Then the photoresist layer was patterned by flood exposure UV light source (Newport model 97436, i-line, 365 nm, 500 W × 3.00 s). The exposed photoresist was immersed in the developer (Shipley MF-319) for 20 s, rinsed with Millipore water (Milli-Q, $p > 18\ M\Omega \cdot cm$), and air-dried. This sample was then exposed to 0.8 M nitric acid for 5 min to remove the nickel and also to produce a horizontal undercut beneath the protective photoresist layer. The height of this undercut was the same as the thickness of the sacrificial nickel layer, and the width of the undercut produced by wet etching was ≈300 nm. The nickel edge of this horizontal trench was used as the working electrode for the electrodeposition of a palladium nanowire.

A 100 mL one-compartment three-electrode electrochemical cell was used for single palladium nanowire electrodeposition. The aqueous plating solution contains 0.2 mM $PdCl_2$, 0.22 mM EDTA, and 0.1 M KCl (adjusted pH = 4.9). The whole photolithographically patterned template was immersed in plating solution while leaving the other edge of nickel out of the plating solution and connected to the potentiostat (Gamry Instrument, model G300). The counter electrode was a precleaned 1 cm^2 platinum foil, and the reference electrode was saturated calomel electrode. Single palladium nanowire was electrodeposited at −0.80 V *vs* SCE. When the electrodeposition was finished, the remaining photoresist layer was dissolved and rinsed off by acetone, and then the nickel layer was etched away by 0.8 M nitric acid, leaving one single palladium nanowire adhering strongly to the glass surface. After the whole LPNE processes, as-made single palladium nanowire samples were thermally treated in nitrogen atmosphere at 200 °C for 2 h by using a heavy duty tube furnace (Lindberg, model 54233).

Fabrication of a Hydrogen Gas Sensor. Quasi-four-probe contacts were made by thermally evaporating Au/Cr (80 nm/2 nm) through a shadow mask with a 50 μm gap on top of the nanowire. Silver paint was applied and sintered at 200 °C to connect Au/Cr contacts to the gas flow cell. For platinum electrodeposition, another layer of photoresist (Shipley S1808) was spun on top of the as-made single nanowire sensor and baked the same as the previous LPNE processes. Then the sample was aligned with a photomask with a rectangle pattern of 25 μm wide and 1 in. long and then shifted horizontally for multiple photolithographic exposures, which were finished by the same flood exposure UV light source. After photoresist development, a single Pd nanowire was exposed as a working electrode for Pt electrodeposition. Then Au/Cr contacts were covered by the photoresist, and Pt electrodeposition on the exposed Pd nanowire was carried out using a three-electrode electrochemical cell. The aqueous plating solution consisted of aqueous 0.1 mM K_2PtCl_6 and 0.1 M KCl.

Scanning Electron Microscopy. Scanning electron micrographs were acquired by using a FEI Magellan 400 XHR system. Energy-dispersive spectroscopic (EDS) images were acquired by same SEM system with an EDS detector (Oxford Instruments, 80 mm^2, with Aztec software). Accelerating voltages of the electron beam ranged from 1 to 5 kV, and probe currents ranged from 1.6 pA to 0.4 nA. All the SEM specimens were mounted on stainless stubs and held by copper clips.

X-ray Photoelectron Spectroscopy. The surface chemical compositions of Pd@Pt nanowires were determined using XPS using a ESCALAB MKII surface analysis instrument (VG Scientific) equipped with a twin anode X-ray source (Mg/Al) and a 150 mm hemispherical electron energy analyzer. XPS spectra were collected under the base pressure of the spectroscopy chamber around 3×10^{-10} Torr using Al Kα with X-ray (1486.6 eV) in constant energy mode, a pass energy of 20 eV, an energy step of 50 meV, and an acquisition time for both Pd 3d and Pt 4f of 3 s. Binding energies were calibrated using the C 1s peak of adventitious carbon at 284.6 eV as a reference and the Au $4f_{7/2}$ at 84.0 eV from gold foil physically attached to the sample surface. Using XPSPEAK software with Shirley-type background functions, Pd 3d XPS spectra were fit with spin−orbit doublets ($3d_{5/2}$ and $3d_{3/2}$) at a fixed intensity ratio (3:2). We assign the features of Pd $3d_{5/2}$ spectra at BE 335.7 eV as metallic Pd and 337.6 eV to Pd^{4+} species, such as PdO_2. Pt 4f XPS spectra were fit with spin−orbit doublets ($4f_{7/2}$ and $4f_{5/2}$) at a fixed intensity ratio (4:3). We assign the features of Pt $4f_{7/2}$ spectra at BE 71.2 eV as metallic Pt and 72.8 eV to Pt^{2+} species, such as PtO or $Pt(OH)_2$. Furthermore, using an atomic sensitivity factor of 5.356 for Pd 3d, 5.575 for Pt 4f, and 0.339 for Si 2p, we further estimate the relative peak concentrations of Pd 3d and Pt 4f normalized to the Si 2p from the glass substrate.

Thermal Calibration. An infrared furnace (ULVAC-RIKO, Inc., model MILA-5000 infrared lamp rapid annealing system) was programmed to ramp temperature in the range of 293 to 393 K. The *in situ* resistance measurement of a 50 μm long single Pd nanowire (40 nm × 200 nm) was determined using a sourcemeter (Keithley Instrument, model 2400) and a multimeter (Keithley Instrument, model 2000) in a nitrogen atmosphere. Sample data are available in the Supporting Information.

Theoretical Simulation. COMSOL Multiphysics (Version 4.3a) was used for finite element modeling of the Joule heating temperature profile along a 50 μm long nanowire (40 nm × 100 nm). The applied module was Joule heating.

Hydrogen Sensing. Single nanowire sensors were mounted in a sealed flow cell (dead volume = 120 μL), equipped with two gas input channels, one for a H_2/air mixture and the other for pure air. The H_2/air mixture was prepared by mixing H_2 with air at known ratios, established by mixing these two gases at controlled gas flow rates produced by mass flow controllers (MKS Inc., model 1479A). Two fast valves (Parker Valve, cycle time = 25 ms) metered pulses of H_2/air into the flow cell and synchronously interrupted the flow of air during the pulse. All hydrogen-sensing experiments were accomplished using dry gases at ambient laboratory temperature (about 20 °C) and a total gas flow rate of 1500 sccm. These two valves and three mass flow controllers were all controlled using LabView in conjunction with a National Instruments interface (model BNC 2110) and a computer. The nanowire resistance was measured in a four-terminal configuration using a combination of a sourcemeter (Keithley Instruments, model 2611A) and a multimeter

(Keithley Instruments, model 2000). The sourcemeter supplied a voltage that fixed the nanowire temperature according to the calibration curve for that particular nanowire (*vide supra*).

Conflict of Interest: The authors declare no competing financial interest.

Acknowledgment. The authors gratefully acknowledge the financial support of this work by the National Science Foundation Division of Chemistry CHE-0956524. Work by Y.L. and J.C.H. was supported by the U.S. Department of Energy, Office of Science, Basic Energy Sciences under Award DE-FG02-96ER45576. SEM data were acquired using instrumentation of the LEXI facility (lexi.eng.uci.edu/) at UCI.

Supporting Information Available: Temperature calibration of Pd@Pt nanowires is described. This material is available free of charge *via* the Internet at http://pubs.acs.org.

REFERENCES AND NOTES

1. Boon-Brett, L.; Bousek, J.; Black, G.; Moretto, P.; Castello, P.; Hübert, T.; Banach, U. Identifying Performance Gaps in Hydrogen Safety Sensor Technology for Automotive and Stationary Applications. *Int. J. Hydrogen Energy* **2010**, *35*, 373–384.
2. Rivkin, C.; Blake, C.; Burgess, R.; Buttner, W. J.; Post, M. B. A National Set of Hydrogen Codes and Standards for the United States. *Int. J. Hydrogen Energy* **2011**, *36*, 2736–2741.
3. Buttner, W. J.; Post, M. B.; Burgess, R.; Rivkin, C. An Overview of Hydrogen Safety Sensors and Requirements. *Int. J. Hydrogen Energy* **2011**, *36*, 2462–2470.
4. Hübert, T.; Boon-Brett, L.; Black, G.; Banach, U. Hydrogen Sensors—A Review. *Sens. Actuators, B* **2011**, *157*, 329–352.
5. Buttner, W.; Burgess, R.; Rivkin, C.; Post, M.; Boon-Brett, L.; Black, G.; Harskamp, F.; Moretto, P. Inter-Laboratory Assessment of Hydrogen Safety Sensors Performance Under Anaerobic Conditions. *Int. J. Hydrogen Energy* **2012**, *37*, 17540–17548.
6. *Funding Opportunity Announcement DE-PS36-09GO99004*; Office of Energy Efficiency and Renewable Energy (EERE), **2009**.
7. Hughes, R. C.; Schubert, W. K. Thin-Films of Pd/Ni Alloys for Detetion of High Hydrogen Concentrations. *J. Appl. Phys.* **1992**, *71*, 542–544.
8. Offermans, P.; Tong, H. D.; van Rijn, C. J. M.; Merken, P.; Brongersma, S. H.; Crego-Calama, M. Ultralow-Power Hydrogen Sensing with Single Palladium Nanowires. *Appl. Phys. Lett.* **2009**, *94*, 223110.
9. Yang, F.; Taggart, D. K.; Penner, R. M. Fast, Sensitive Hydrogen Gas Detection Using Single Palladium Nanowires That Resist Fracture. *Nano Lett.* **2009**, *9*, 2177–2182.
10. Yang, F.; Taggart, D.; Penner, R. Joule-Heating a Palladium Nanowire Sensor for Accelerated Response and Recovery to Hydrogen Gas. *Small* **2010**, *6*, 1422–1429.
11. Yang, F.; Kung, S.-C.; Cheng, M.; Hemminger, J. C.; Penner, R. M. Smaller Is Faster and More Sensitive: The Effect of Wire Size on the Detection of Hydrogen by Single Palladium Nanowires. *ACS Nano* **2010**, *4*, 5233–5244.
12. Yang, F.; Kung, S.-C.; Taggart, D. K.; Penner, R. M. Hydrogen Sensing with a Single Palladium Nanowire. *Sensor Lett.* **2010**, *8*, 534–538.
13. Yang, F.; Donavan, K. C.; Kung, S.-C.; Penner, R. M. The Surface Scattering-Based Detection of Hydrogen in Air Using a Platinum Nanowire. *Nano Lett.* **2012**, *12*, 2924–2930.
14. Favier, F.; Walter, E.; Zach, M.; Benter, T.; Penner, R. Hydrogen Sensors and Switches from Electrodeposited Palladium Mesowire Arrays. *Science* **2001**, *293*, 2227–2231.
15. Walter, E.; Penner, R.; Liu, H.; Ng, K.; Zach, M.; Favier, F. Sensors from Electrodeposited Metal Nanowires. *Surf. Interface Anal.* **2002**, *34*, 409–412.
16. Walter, E.; Favier, F.; Penner, R. Palladium Mesowire Arrays for Fast Hydrogen Sensors and Hydrogen-Actuated Switches. *Anal. Chem.* **2002**, *74*, 1546–1553.
17. Xu, T.; Zach, M.; Xiao, Z.; Rosenmann, D.; Welp, U.; Kwok, W.; Crabtree, G. Self-Assembled Monolayer-Enhanced Hydrogen Sensing with Ultrathin Palladium Films. *Appl. Phys. Lett.* **2005**, *86*, 203104.
18. Zeng, X.; Latimer, M.; Xiao, Z.; Panuganti, S.; Welp, U.; Kwok, W.; Xu, T. Hydrogen Gas Sensing with Networks of Ultrasmall Palladium Nanowires Formed on Filtration Membranes. *Nano Lett.* **2010**, *11*, 262–268.
19. Kaltenpoth, G.; Schnabel, P.; Menke, E.; Walter, E.; Grunze, M.; Penner, R. Multimode Detection of Hydrogen Gas Using Palladium-Covered Silicon μ-Channels. *Anal. Chem.* **2003**, *75*, 4756–4765.
20. Zeng, X.-Q.; Wang, Y.-L.; Deng, H.; Latimer, M. L.; Xiao, Z.-L.; Pearson, J.; Xu, T.; Wang, H.-H.; Welp, U.; Crabtree, G. W.; et al. Networks of Ultrasmall Pd/Cr Nanowires as High Performance Hydrogen Sensors. *ACS Nano* **2011**, *5*, 7443–7452.
21. Kiefer, T.; Favier, F.; Vazquez-Mena, O.; Villanueva, G.; Brugger, J. A Single Nanotrench in a Palladium Microwire for Hydrogen Detection. *Nanotechnology* **2008**, *19*, 125502.
22. Kiefer, T.; Villanueva, L.; Fargier, F.; Favier, F.; Brugger, J. Fast and Robust Hydrogen Sensors Based on Discontinuous Palladium Films on Polyimide, Fabricated on a Wafer Scale. *Nanotechnology* **2010**, *21*, 505501.
23. Lee, J.; Shim, W.; Lee, E.; Noh, J.-S.; Lee, W. Highly Mobile Palladium Thin Films on an Elastomeric Substrate: Nanogap-Based Hydrogen Gas Sensors. *Angew. Chem., Int. Ed.* **2011**, *123*, 5413–5417.
24. Lewis, F. A. *The Palladium Hydrogen System*; Academic Press: London, 1967.
25. Gland, J.; Sexton, B.; Fisher, G. Oxygen Interactions with the Pt(111) Surface. *Surf. Sci.* **1980**, *95*, 587–602.
26. Fisher, G.; Gland, J. The Interaction of Water with the Pt(111) Surface. *Surf. Sci.* **1980**, *94*, 446–455.
27. Ogle, K.; White, J. The Low-Temperature Water Formation Reaction of Pt(111)—A Static SIM and TDS Study. *Surf. Sci.* **1984**, *139*, 43–62.
28. Johansson, M.; Ekedahl, L. Hydrogen Adsorbed on Palladium during Water Formation Studied with Palladium Membranes. *Appl. Surf. Sci.* **2001**, *173*, 122–133.
29. Xiang, C.; Yang, Y.; Penner, R. M. Cheating the Diffraction Limit: Electrodeposited Nanowires Patterned by Photolithography. *Chem. Commun.* **2009**, 859–873.
30. Gokcen, D.; Bae, S.-E.; Brankovic, S. R. Stoichiometry of Pt Submonolayer Deposition *via* Surface-Limited Redox Replacement Reaction. *J. Electrochem. Soc.* **2010**, *157*, D582–D587.
31. Fayette, M.; Liu, Y.; Bertrand, D.; Nutariya, J.; Vasiljevic, N.; Dimitrov, N. From Au to Pt *via* Surface Limited Redox Replacement of Pb UPD in One-Cell Configuration. *Langmuir* **2011**, *27*, 5650–5658.
32. Nutariya, J.; Fayette, M.; Dimitrov, N.; Vasiljevic, N. Growth of Pt by Surface Limited Redox Replacement of Underpotentially Deposited Hydrogen. *Electrochim. Acta* **2013**, *112*, 813–823.
33. Sun, Y.; Xia, Y. Alloying and Dealloying Processes Involved in the Preparation of Metal Nanoshells through a Galvanic Replacement Reaction. *Nano Lett.* **2003**, *3*, 1569–1572.
34. Chen, J.; Wiley, B.; McLellan, J.; Xiong, Y.; Li, Z.-Y.; Xia, Y. Optical Properties of Pd—Ag and Pt—Ag Nanoboxes Synthesized *via* Galvanic Replacement Reactions. *Nano Lett.* **2005**, *5*, 2058–2062.
35. Vasilic, R.; Viyannalage, L.; Dimitrov, N. Epitaxial Growth of Ag on Au (111) by Galvanic Displacement of Pb and Ti Monolayers. *J. Electrochem. Soc.* **2006**, *153*, C648–C655.
36. Zangwill, A. *Physics at Surfaces*; Cambridge University Press: Cambridge, U.K., 1988.
37. Gu, S.; Wang, X.; Wei, Y.; Fang, B. Mechanism for Nucleation and Growth of Electrochemical Deposition of Palladium (II) on a Platinum Electrode in Hydrochloric Acid Solution. *Sci. China Chem.* **2014**, *57*, 755–762.
38. Naohara, H.; Ye, S.; Uosaki, K. Electrochemical Layer-by-Layer Growth of Palladium on an Au (111) Electrode Surface: Evidence for Important Role of Adsorbed Pd Complex. *J. Phys. Chem. B* **1998**, *102*, 4366–4373.
39. Palomar-Pardave, M.; González, I.; Batina, N. New Insights into Evaluation of Kinetic Parameters for Potentiostatic

Metal Deposition with Underpotential and Overpotential Deposition Processes. *J. Phys. Chem. B* **2000**, *104*, 3545–3555.
40. Gunawardena, G.; Hills, G.; Montenegro, I.; Scharifker, B. Electrochemical Nucleation: Part I. General Considerations. *J. Electroanal. Chem. Interfacial Electrochem.* **1982**, *138*, 225–239.
41. Scharifker, B.; Hills, G. Theoretical and Experimental Studies of Multiple Nucleation. *Electrochim. Acta* **1983**, *28*, 879–889.
42. Scharifker, B.; Mostany, J. Three-Dimensional Nucleation with Diffusion Controlled Growth: Part I. Number Density of Active Sites and Nucleation Rates Per Site. *J. Electroanal. Chem. Interfacial Electrochem.* **1984**, *177*, 13–23.
43. Grigoriev, S.; Millet, P.; Fateev, V. Evaluation of Carbon-Supported Pt and Pd Nanoparticles for the Hydrogen Evolution Reaction in PEM Water Electrolysers. *J. Power Sources* **2008**, *177*, 281–285.
44. Grigoriev, S. A.; Fateev, V. N.; Middleton, H.; Saetre, T. O. A Comparative Evaluation of Palladium and Platinum Nanoparticles as Catalysts in Proton Exchange Membrane Electrochemical Cells. *Int. J. Nucl. Hydrogen. Prod. Appl.* **2008**, *1*, 343–354.
45. Rand, D.; Woods, R. A Study of the Dissolution of Platinum, Palladium, Rhodium and Gold Electrodes in 1 M Sulphuric Acid by Cyclic Voltammetry. *J. Electroanal. Chem. Interfacial Electrochem.* **1972**, *35*, 209–218.
46. Jeon, K. J.; Jeun, M.; Lee, E.; Lee, J. M.; Lee, K.-I.; von Allmen, P.; Lee, W. Finite Size Effect on Hydrogen Gas Sensing Performance in Single Pd Nanowires. *Nanotechnology* **2008**, *19*, 495501.
47. Jeon, K. J.; Lee, J. M.; Lee, E.; Lee, W. Individual Pd Nanowire Hydrogen Sensors Fabricated by Electron-Beam Lithography. *Nanotechnology* **2009**, *20*, 135502.
48. Wicke, E.; Brodowsky, H.; Alefeld, G.; Völkl, J. Hydrogen in Metals II. *Top. Appl. Phys.* **1978**, *29*, 73.
49. Lewis, F. Hydrogen in Palladium and Palladium Alloys. *Int. J. Hydrogen Energy* **1996**, *21*, 461–464.